Effects of Molecular Geometry on the STM Image Contrast of Methyl- and Bromo-Substituted Alkanes and Alkanols on Graphite

Christopher L. Claypool, Francesco Faglioni, Adam J. Matzger, William A. Goddard III,* and Nathan S. Lewis*

Division of Chemistry and Chemical Engineering, California Institute of Technology, Pasadena, California 91125

Received: July 1, 1999; In Final Form: August 27, 1999

Scanning tunneling microscopy (STM) images have been collected for a series of substituted alkanes and alkanols that form ordered overlayers at room temperature on highly ordered pyrolytic graphite surfaces. Molecules that have been imaged possess an internal bromide, with or without terminal alcohol groups ($HO(CH_2)_9CHBr(CH_2)_{10}OH$ and $H_3C(CH_2)_{16}CHBr(CH_2)_{16}CH_3$), an internal −OH group ($H_3C(CH_2)_{16}CHOH(CH_2)_{16}CH_3$), and an internal methyl group ($H_3C(CH_2)_{16}CHCH_3(CH_2)_{16}CH_3$). These data allow comparison to the STM image contrast reported previously for molecules in which −OH, −Br, and $-CH_3$ groups were located in terminal positions of alkane chains adsorbed onto graphite surfaces. When the functional groups were in gauche positions relative to the alkyl chain, and thus produced molecular features that protruded toward the tip, the functional groups were observed to produce bright regions in a constant current STM image, regardless of the STM contrast behavior observed for these same functional groups when they were in terminal positions of adsorbed alkyl chains. These observations are in excellent agreement with theoretical predictions of the STM behavior of such systems. Additionally, several interesting packing structures have been observed that have yielded insight into the intermolecular forces that control the packing displayed by these overlayers.

I. Introduction

Various laboratories have now reported scanning tunneling microscopy (STM) images that appear to reveal the internal structure of molecules.[1−20] Unlike optical microscopy, where knowledge of the spatial variation in the values of the real and imaginary components of the refractive index allows computation of the image contrast between adjacent regions of an interfacial layer, the fundamental mechanisms that produce the contrast in a STM image remain to be fully elucidated.[21−25] In general, variations in both topographic and electronic properties of a molecular overlayer will influence the contrast of an STM image. To date, the relative role of these factors remains largely unexplored experimentally.

A particularly attractive system for the investigation of these questions involves imaging alkanes or alkanols that are adsorbed onto highly ordered pyrolytic graphite (HOPG) surfaces.[21−35] These species produce ordered overlayers that allow resolution of various atomic and functional group features using STM.[21−35] In addition, systematic changes in the topographic and electronic structure of these molecules can be correlated with changes in the observed STM images.[21−35]

In prior work, the interplay between topographic and electronic considerations was seen to be critical to determining the local contrast of STM images of various functional groups in alkane and alkanol overlayers on graphite. For example, relative to a "reference" methylene region of the molecule, the larger but poorer-coupling $-CF_3$ groups were dark in STM images, whereas double and triple bonds, with their π systems, produced locally bright regions in STM images.[25] In some cases, changes in the topographic parameters were predicted to change the sign of the image contrast of a given functional group. For example, a terminal −Br group in straight-chain α,ω alkanol bromides was observed to be dark relative to the alkyl chain.[26] This was believed to be due to poorer electronic coupling of the −Br group relative to the alkyl chain when the −Br is in the trans conformation and when the alkyl chain is oriented such that its carbon−carbon skeleton is parallel to the graphite surface plane. Theoretical calculations, however, predict that because of the dominant influence of topography, if the terminal −Br were in a gauche position and all other factors were constant, the −Br group would produce a bright region in the STM image.[25] Similarly, terminal −OH groups in straight-chain alkanol

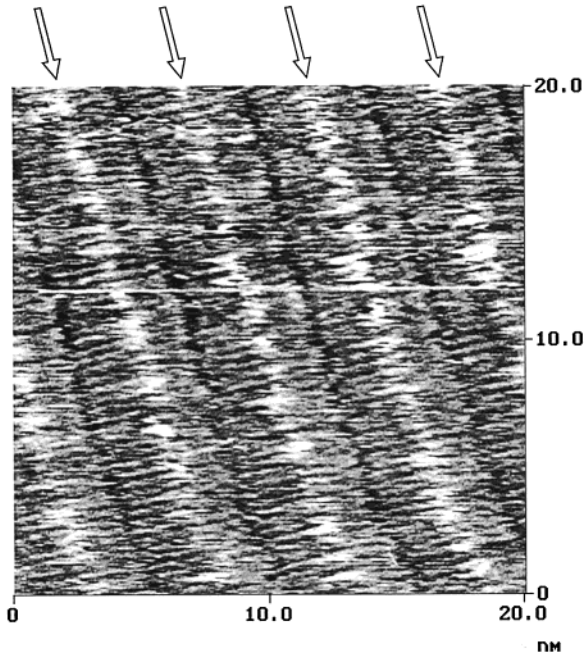

Figure 1. STM image of $H_3C(CH_2)_{16}CHOH(CH_2)_{16}CH_3$ molecules on graphite ($V = 1.210$ V, $I = 200$ pA). The bright region in the middle of the molecular rows is assigned to the hydroxyl functionality (white arrows).

10.1021/jp992257t CCC: $18.00
Published on Web 10/15/1999

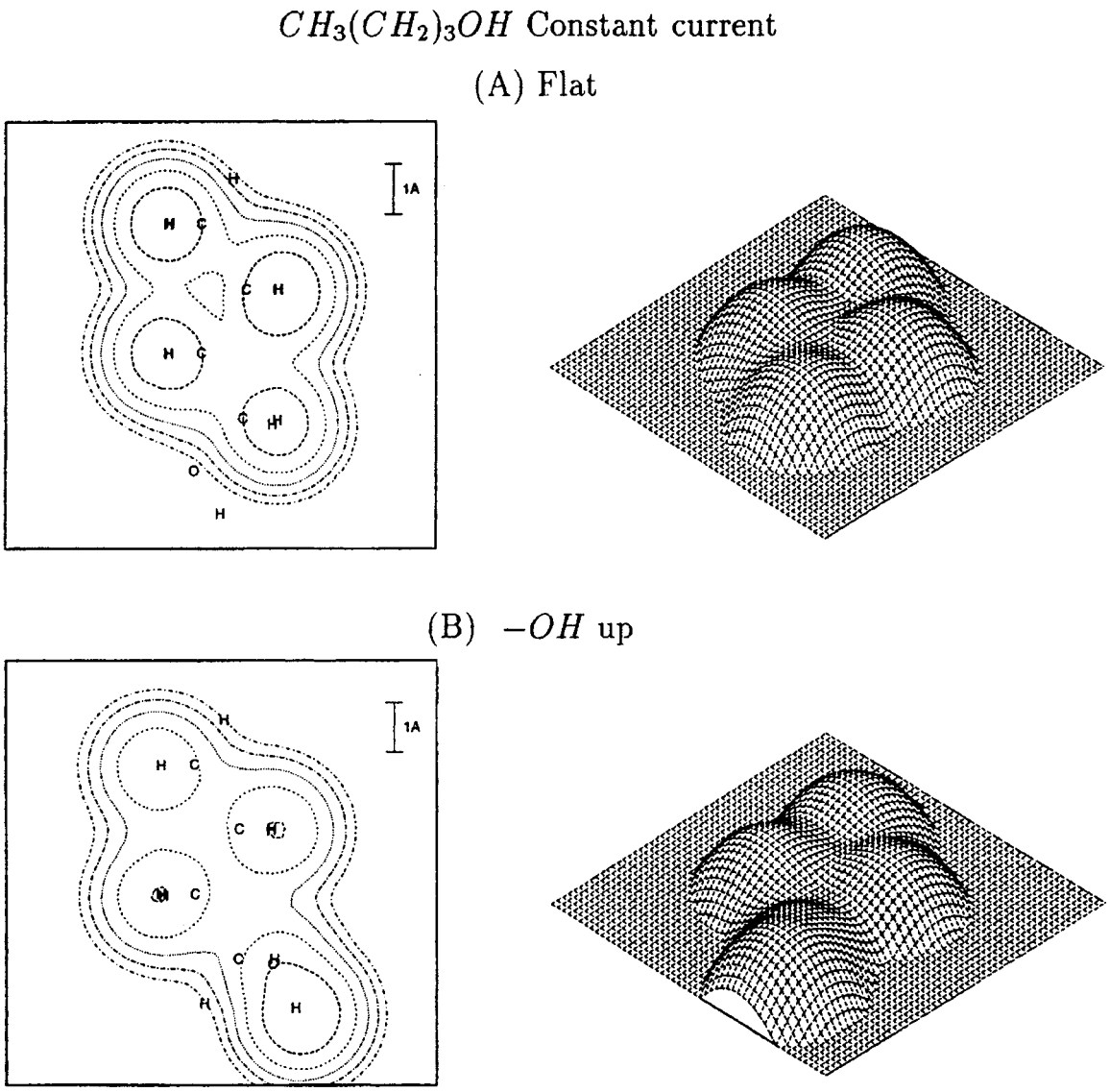

Figure 2. (A) Calculated constant-current STM image for an alcohol molecule laid flat on the graphite surface with the terminal OH group in a position trans to the alkyl chain (flat on the graphite) and (B) gauche to the alkyl chain (pointing away from the graphite). Molecular modeling of $CH_3(CH_2)_5CHOH(CH_2)_5CH_3$ indicated that the −OH group was 0.9 Å higher than the methylene portion of the molecule, while the STM simulation in part B produced a 0.06 Å protrusion over the region of the −OH group.

overlayers were observed to be dark relative to the reference methylene chain regions, but such terminal −OH groups are predicted computationally to be bright if they are instead located in gauche conformations relative to the carbon−carbon chain.[25]

This work describes the results of a series of experiments that have been designed to address further the interplay between topographic and electronic factors in an STM image. Bromide, −OH, and $-CH_3$ groups have been placed at internal positions in an alkane chain; in addition, a −Br group has been located internally on a long-chain α,ω diol. STM images of overlayers of these molecules on HOPG have revealed the location of, and the image contrast displayed by, all of these functional groups. In addition, several interesting packing arrangements have been identified for these molecules, and the variation in packing has yielded insight into the intermolecular forces that determine the packing arrangements exhibited by two-dimensional ordered overlayers.

II. Experimental Section

A. Methods. Sample preparation and imaging conditions were similar to those reported previously.[24] Briefly, samples were prepared by placing a 6 μL droplet of a concentrated solution of the organic compound in phenyloctane onto a freshly cleaved highly ordered pyrolytic graphite (HOPG, Union Carbide) surface. A mechanically formed Pt−Ir tip was then immersed in the liquid droplet, and the imaging was performed at the liquid−graphite interface. Images were obtained using a Digital Instruments (Santa Barbara, CA) Nanoscope III STM. All of the images presented herein were obtained at constant current in the variable height mode. Bright portions of the images correspond to points at which the tip retracted from the surface in order to maintain a constant current.

The lattice spacing of graphite (2.46 Å) was used as the calibration standard for the *x* and *y* piezo dimensions. Step edges observed on an oxidized graphite surface[36] (3.35 Å) were used as a calibration standard for the *z* piezo dimension. Distances and angles were determined using Nanoscope III software, and the apparent heights of heteroatoms and functional groups are reported with respect to the average height of the image over the methylene portion of the adsorbed molecule. Errors in the distances quoted in this manuscript include estimates of the measurement errors associated with determining the metrics

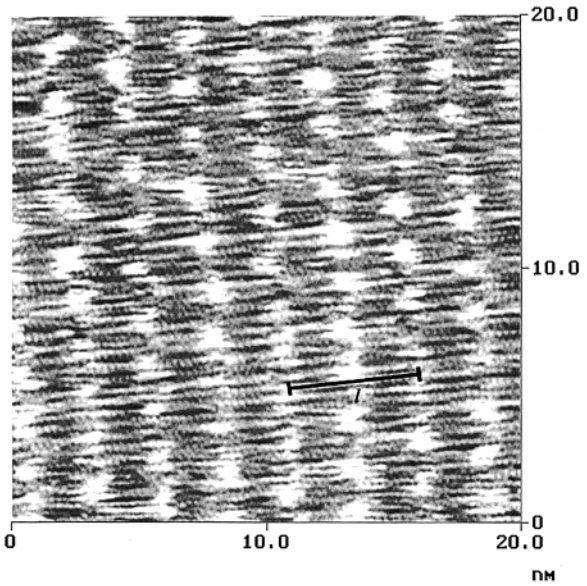

Figure 3. STM image of $H_3C(CH_2)_{16}CHCH_3(CH_2)_{16}CH_3$ molecules on graphite ($V = 1.351$ V, $I = 200$ pA). The bright regions are assigned to the internal methyl groups.

from the images as well as variation in the metrics over various experiments. To reduce noise, the images were filtered using Nanoscope III software. The filtering was primarily performed to enhance the visual presentation of the printed images, but the filtering was performed in such a way that it did not distort any of the primary metrics evident in the original data. The filtering procedure also did not introduce any new spot patterns or new topographic features into an image.

Images similar to those reported in this work were obtained many times in several different imaging sessions. In all cases, similar images were observed at many different locations on a sample. Nearly every sample yielded evidence of the adsorbed monolayer in the STM image; however, several different tips were usually necessary to achieve the high-resolution images reported in this work.

Numerical simulations of the STM images of adsorbates were performed as described previously.[25] First, the adsorbate geometry was estimated using the DreidingII force field[37] by placing one molecular monolayer on graphite. The position of the adsorbed molecules was optimized on the original graphite plane using a DreidingII force field. Since there are no explicit bonds between graphite and the adsorbates, the position of the adsorbate is determined mainly by van der Waals interactions. This results in the adsorbate's carbon backbone being as staggered as possible with respect to the graphite carbons and with the hydrogens of the absorbate resting on top of the surface hexagons. Then one molecule from the monolayer was selected and the alkyl chains were truncated three or four carbon atoms away from the functional group of interest. The dangling bonds of the fragment were saturated with hydrogen atoms, but the geometry of the fragment was otherwise preserved. Then a gas-phase Hartree−Fock computation was performed on the fragment using the commercial Gaussian package.[38] The force field geometry and Hartree−Fock wave function were then used to estimate the perturbative coupling of the tip and the graphite states. In the STM simulation the graphite was replaced with a finer rectangular grid of orbitals in order to minimize the effect of lateral displacements of the adsorbates that may occur in the real system. As a consequence, different arrangements of the molecules with respect to the graphite lattice have very little effect on the simulated STM images as long as the molecular geometry is not changed significantly (e.g., going from a flat to a vertical orientation). The coupling, which is related to the tunneling current, was computed using a simple model that contained only one adjustable parameter.[25] The value of this parameter was fixed to be the same as that used previously.[25] The vertical position of the model tip was then adjusted to maintain a constant current at every point on a rectangular grid that covered the adsorbed fragment. The optimal tip height was recorded and used to produce simulated constant-current images.

The data from the simulations are reported both as three-dimensional surfaces, representing the vertical tip displacement with respect to an arbitrary zero, and as contour plots. The contour levels are $^1/_6$, $^2/_6$, $^3/_6$, $^4/_6$, and $^5/_6$, respectively, of the maximum peak of each plot.

B. Materials. Stearone (TCI) and phenyloctane (Aldrich) are commercially available and were used as received. The proce-

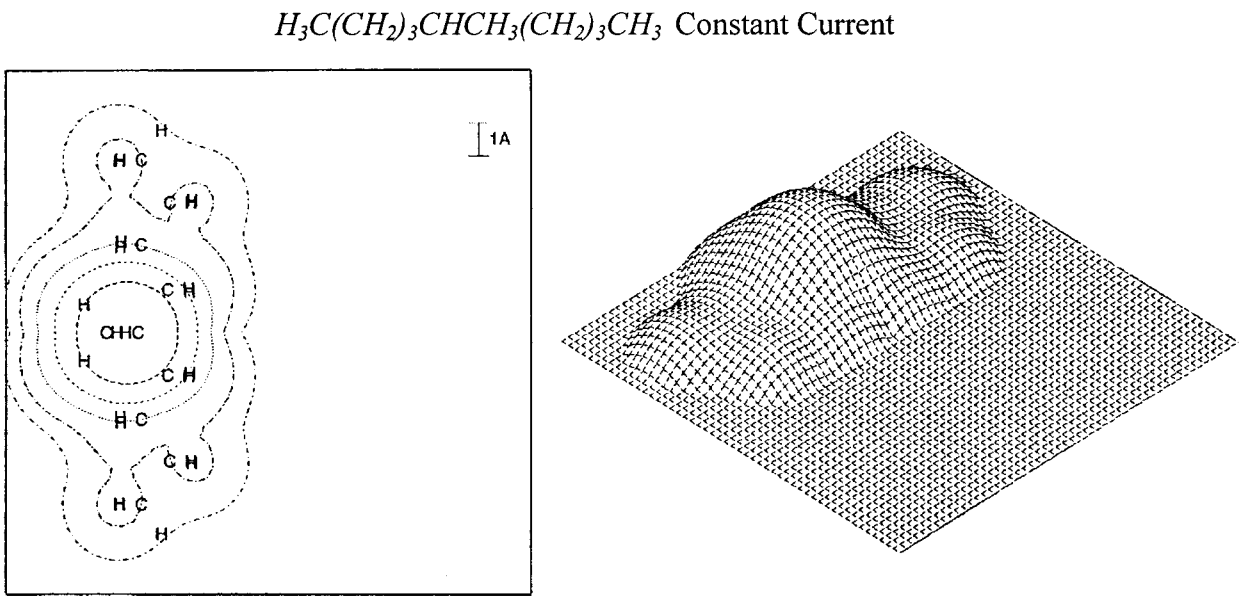

Figure 4. Calculated constant-current STM image for a methyl alkane molecule laid flat on the graphite surface with the internal methyl group in a position pointing away from the graphite surface. Molecular modeling of $H_3C(CH_2)_{16}CHCH_3(CH_2)_{16}CH_3$ indicated that the internal methyl group is 1.7 Å higher than the methylene backbone of the molecule, while the STM simulation shown in the figure produces a 1.58 Å peak over the region of the internal methyl group.

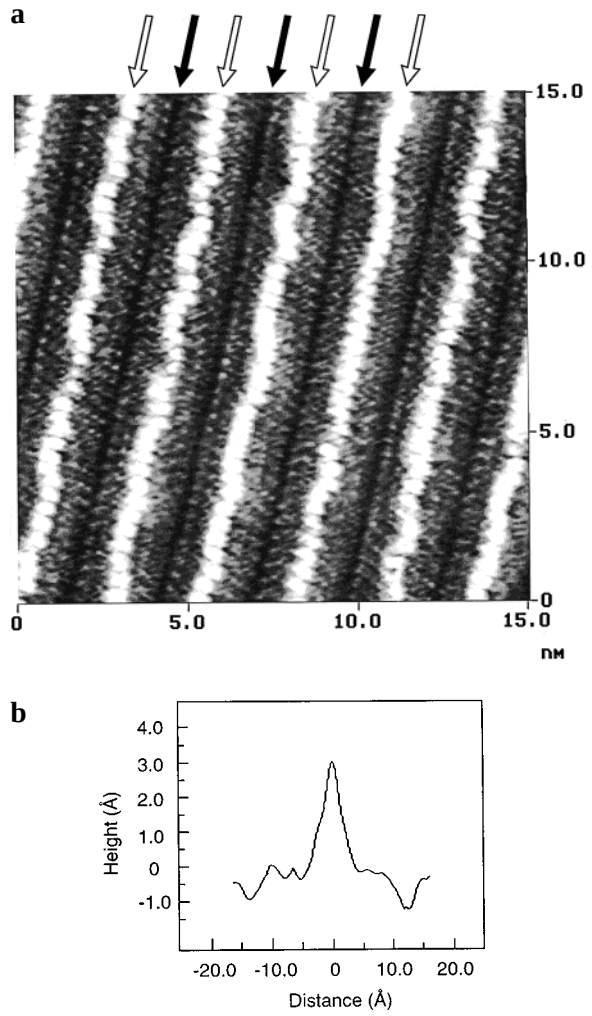

Figure 5. (a) STM image of $HO(CH_2)_9CHBr(CH_2)_{10}OH$ molecules on graphite ($V = 1.061$ V, $I = 200$ pA). The black arrows indicate the dark troughs associated with the terminal hydroxyl groups, and the bright regions (white arrows) are assigned to the internal bromine atoms. (b) Single line scan along the length of a molecule. Note the asymmetric location of the peak assigned to the bromine atom relative to the location of the troughs assigned to the terminal hydroxyl groups.

dures used to prepare and purify the other compounds imaged in this work are described below.

Synthesis of $H_3CO_2C(CH_2)_9CH{=}CH(CH_2)_9CO_2CH_3$. Methyl undecylenate (2.58 g, 13.0 mmol) was treated with $(PCy_3)_2Cl_2Ru{=}CHPh$ (108 mg, 0.132 mmol) (Cy = cyclohexyl) and vigorously stirred under vacuum for 5 h. Filtration of the crude reaction mixture through silica gel eluting with 25% EtOAc in hexanes afforded 2.33 g (97%) of dimethyl eicos-10-ene-1,20-dicarboxalate as a mixture of isomers. Further purification was achieved by recrystallization from methanol. ^{1}H NMR ($CDCl_3$): δ 1.27 (s, 20 H), 1.61 (t, 4 H), 1.91−1.98 (m, 4 H), 2.30 (t, 4 H), 3.66 (s, 6 H), 5.37 (t, 2 H).

Synthesis of $H_3CO_2C(CH_2)_9CHBr(CH_2)_{10}CO_2CH_3$. Dimethyl eicos-10-ene-1,20-dicarboxylate (0.415 g, 1.13 mmol) was dissolved in acetic acid (10 mL) and treated with HBr in acetic acid (4.0 mL of a 30% solution). The product was isolated by pouring the solution into water after 6 h. The oil formed was recovered from the aqueous layer by extraction with ether/hexanes (1:1) and was then dried over anhydrous Na_2SO_4. Concentration afforded an oil (0.320 g) that was used crude in the next step.

Synthesis of $HO(CH_2)_9CHBr(CH_2)_{10}OH$. Dimethyl 10-bromoeicosane-1,20-dicarboxylate was dissolved in dry CH_2Cl_2 (20 mL) and cooled in an ice bath. Diisobutylaluminum hydride (7.0 mL of a 1.0 M solution in THF) was added to this solution dropwise over 10 min. After 4.5 h, the reaction was quenched by slow addition of methanol (3.0 mL) and 10 min of stirring followed by the addition of 1 M HCl (10 mL). The solution was warmed to room temperature, and more 1 M HCl (30 mL) was added. The organic layer was separated, washed with brine (50 mL), and dried over anhydrous Na_2SO_4. Removal of the solvent yielded an oil that solidified upon standing (0.314 g, 71% for two steps). Further purification was achieved by crystallization from CH_2Cl_2−hexanes at −6 °C to give a white powder. Anal. Calcd for $C_{20}H_{41}BrO_2$: C, 61.06; H, 10.50. Found: C, 61.51; H, 10.19.

Synthesis of $CH_3(CH_2)_{16}CHOH(CH_2)_{16}CH_3$. Stearone (3.00 g, 5.92 mmol) and $LiAlH_4$ (0.339 g, 8.93 mmol) were dissolved in THF (200 mL) and stirred for 3 days. Excess reducing agent was quenched by sequential addition of water (0.30 mL), 10% NaOH solution (0.45 mL), and water (0.90 mL). The resulting salts were filtered off on a fritted funnel and the product recovered from the filtrate by evaporation (0.612 g, 20%), mp 77.5−80.0 °C. ^{1}H NMR ($CDCl_3$): δ 0.88 (t, 6 H), 1.25 (s, 60 H), 1.55 (br s, 4H), 3.58 (br s, 1 H). Anal. Calcd for $C_{35}H_{72}O$: C, 82.60; H, 14.26. Found: C, 82.85; H, 14.13.

Synthesis of $CH_3(CH_2)_{16}CHBr(CH_2)_{16}CH_3$. PPh_3 (1.29 g, 4.94 mmol) and Br_2 (250 μL, 4.85 mmol) were added to 18-pentatriacontanol (0.528 g, 1.04 mmol) suspended in dry THF (75 mL). After 20 h, methanol (0.75 mL) was added and the solvent was removed under reduced pressure. Purification by column chromatography on silica gel with hexanes as eluent provided a colorless oil that solidified upon standing. Further purification was achieved by crystallization from ethanol/CH_2Cl_2 (3:1) to afford a white powder (0.3875 g, 65%), mp 44−45.5 °C. ^{1}H NMR ($CDCl_3$): δ 0.88 (t, 6 H), 1.25 (s, 60 H), 1.79 (m, 4 H), 4.03 (q, 1 H). Anal. Calcd for $C_{35}H_{71}Br$: C, 73.51; H, 12.51. Found: C, 74.45; H, 12.52.

Synthesis of $CH_3(CH_2)_{16}(CCH_2)(CH_2)_{16}CH_3$. Butyllithium (5.60 mL of a 1.6 M solution in hexanes, 8.96 mmol) was added to a solution of methyltriphenylphosphonium bromide (3.67 g, 10.3 mmol) in THF (100 mL). After 5 min, stearone (1.50 g, 2.96 mmol) was added and the solution was stirred for 3 days. Excess reagent was quenched by addition of acetone (1.5 mL), and the solvent was removed under reduced pressure. Pure product was obtained after chromatography on silica gel eluting with hexanes followed by evaporation of the solvent (1.13 g, 76%), mp 53.5−55 °C. ^{1}H NMR ($CDCl_3$): δ 0.88 (t, 6 H), 1.25 (s, 60 H), 2.01 (t, 4 H), 5.45 (br s, 2 H). Anal. Calcd for $C_{36}H_{72}$: C, 85.63; H, 14.37. Found: C, 85.68; H, 14.45.

Synthesis of $CH_3(CH_2)_{16}CHCH_3(CH_2)_{16}CH_3$. The alkene (0.190 g, 0.375 mmol) and 10% Pd−C (20.5 mg) were suspended in THF (50 mL) and kept under a hydrogen atmosphere for 1 day. The product was recovered after filtration through silica gel eluting with hexanes and concentration of the resulting filtrate, mp 48.5−49 °C. ^{1}H NMR ($CDCl_3$): δ 0.83 (d, 3 H), 0.88 (t, 6 H), 1.25 (s, 65 H). Anal. Calcd for $C_{36}H_{74}$: C, 85.29; H, 14.71. Found: C, 85.68; H, 14.45.

III. Results

1. STM Images of $H_3C(CH_2)_{16}CHOH(CH_2)_{16}CH_3$. Figure 1 presents an STM image of an alkane having an internal hydroxyl functionality, 18-hydroxy-pentatriacontane, $H_3C(CH_2)_{16}CHOH(CH_2)_{16}CH_3$. The mean molecular length in the image is 46.7 ± 0.5 Å, compared to molecular modeling predictions of a molecular length of 45.5 Å for the all-trans conformation of $H_3C(CH_2)_{16}CHOH(CH_2)_{16}CH_3$. Features that are assigned to hydroxyl groups (white arrows) appear bright relative to the

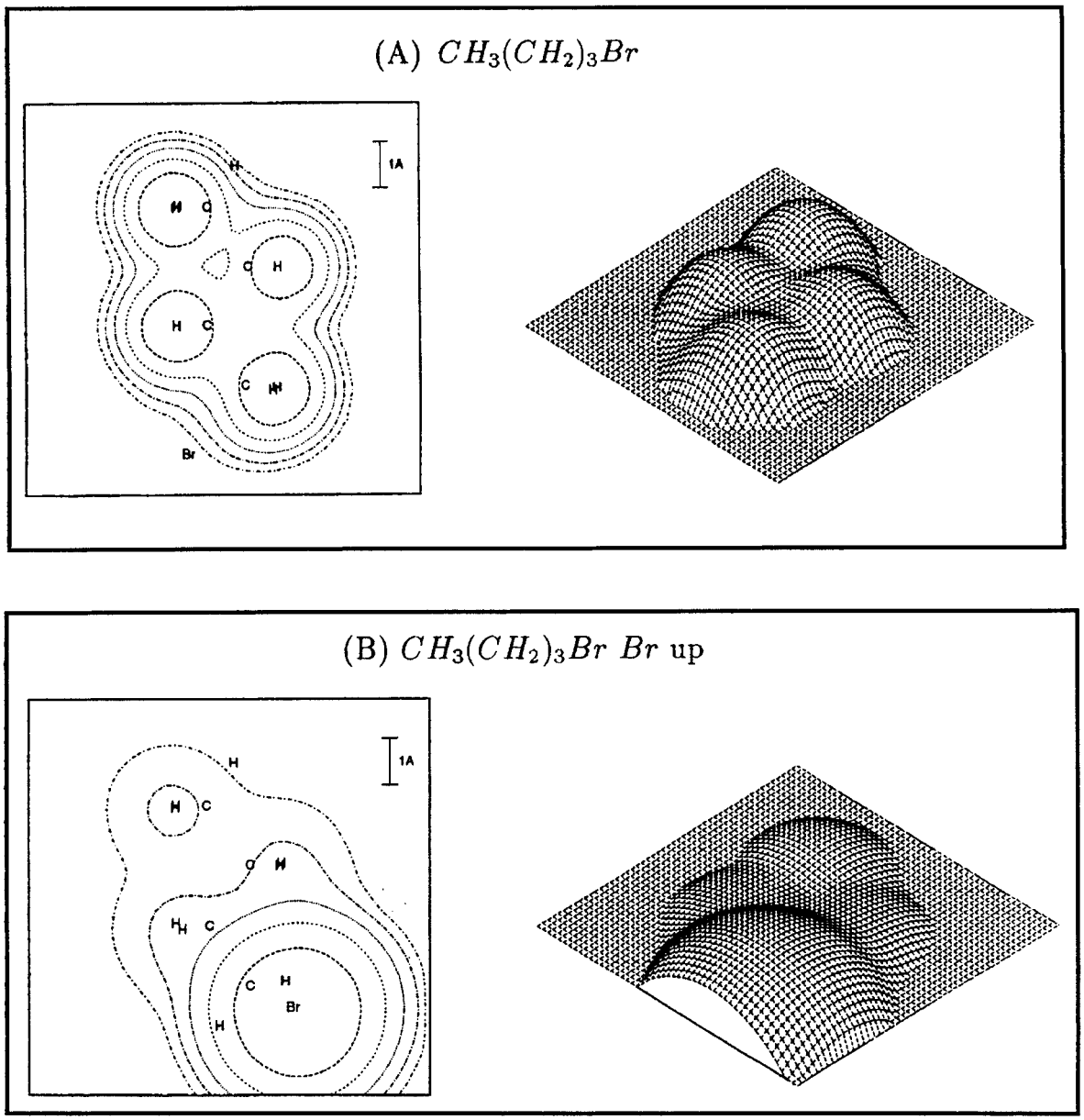

Figure 6. (A) Calculated constant-current STM image for a terminal bromine atom in a position trans to the alkyl chain (flat on the graphite) and (B) gauche to the alkyl chain (pointing away from the graphite).

methylene units and have an average length of 9.0 ± 0.5 Å and an average height of 0.30 ± 0.05 Å. The molecules are ordered in a parallel arrangement, with the packing angle θ defined as the angle between the vector parallel to an alkyl chain and the vector perpendicular to the propagation direction of a lamella, equal to 0°. Adjacent molecules in abutting lamellae stagger by $^1/_2$ a molecular width.

The STM image contrast displayed by the −OH group clearly depends on its geometric orientation in the molecule. Terminal alcohols in $C_{10}H_{21}OH$, $C_{12}H_{25}OH$, $C_{14}H_{29}OH$, 1,12-dodecanediol, 1,14-tetradecanediol, $CF_3(CH_2)_{11}OH$, $CF_3(CF_2)_3(CH_2)_{10}OH$, $Br(CH_2)_{11}OH$, $Br(CH_2)_{12}OH$, $Cl(CH_2)_{12}OH$, $I(CH_2)_{12}OH$, $H_3C(CH_2)_7C{\equiv}C(CH_2)_6OH$, and $HO(CH_2)_{12}C{\equiv}N$ overlayers on graphite[21−24] have been observed to produce dark −OH regions relative to the methylene regions of these molecules. In contrast, the calculated images for the situation in which the −OH group points away from the graphite (gauche to the alkyl chain) indicate that the −OH group should be slightly brighter in an STM image than the surrounding methylene units (Figure 2). This prediction is in excellent agreement with the experimental observations for $H_3C(CH_2)_{16}CHOH(CH_2)_{16}CH_3$ (Figure 1), whose internal −OH group must obviously be in a gauche conformation relative to the alkyl chain.

2. STM Images of $H_3C(CH_2)_{16}CHCH_3(CH_2)_{16}CH_3$. The STM image of an alkane having an internal methyl functionality, 18-methylpentatriacontane, $H_3C(CH_2)_{16}CHCH_3(CH_2)_{16}CH_3$, is shown in Figure 3. The average length of the molecules is 46.3 ± 0.5 Å, which is in good agreement with the expected length of 45.6 Å that is obtained from molecular modeling of the all-trans comformation of $H_3C(CH_2)_{16}CHCH_3(CH_2)_{16}CH_3$. The packing angle is the same as that observed for other alkanes, with $\theta = 0°$. However, in contrast to the behavior observed for alkane overlayers on HOPG and in contrast to the packing of $H_3C(CH_2)_{16}CHOH(CH_2)_{16}CH_3$ (Figure 1), the $H_3C(CH_2)_{16}CHCH_3(CH_2)_{16}CH_3$ molecules do not stagger perpendicular to the propagation direction of a lamella by $^1/_2$ a molecular width. Instead, within observational accuracy, adjacent molecules in abutting lamellae are collinear.

The bright features in the image have a mean length of 10.9 ± 0.5 Å and a mean height of 0.74 ± 0.05 Å. These features

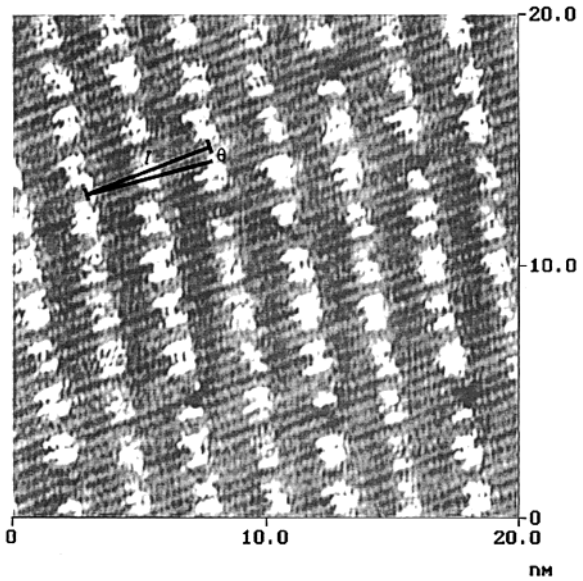

Figure 7. STM image of $H_3C(CH_2)_{16}CHBr(CH_2)_{16}CH_3$ molecules on graphite ($V = 1.304$ V, $I = 200$ pA). The bright regions correspond to the bromine heteroatoms.

are attributed to the internal methyl groups. Calculations indicate that topographical effects should make the methyl group bright relative to the surrounding methylene units (Figure 4), and this prediction is in excellent agreement with the experimental results.

3. STM Images of $HO(CH_2)_9CHBr(CH_2)_{10}OH$. An STM image of 10-bromo-1,20-eicosanediol, $HO(CH_2)_9CHBr(CH_2)_{10}OH$, is shown in Figure 5a. The average length of the molecules is 28.4 ± 0.2 Å, which is in excellent agreement with the length of 28.3 Å obtained from molecular modeling for the all-trans conformation of $HO(CH_2)_9CHBr(CH_2)_{10}OH$. The molecules display a molecular packing angle of $\theta = 23°$ and thus appear to be ordered in the herringbone fashion exhibited by unsubstituted alkanols.

The terminal −OH groups are identifiable as troughs of length 3.5 ± 0.1 Å and depth -0.61 ± 0.05 Å (black arrows). The bright feature that is centered 14.7 Å from one end of the molecule and 13.5 Å from the other (Figure 5) is assigned to the Br− functionality. This bright feature has an average length of 8.8 ± 0.2 Å and a mean height of 3.11 ± 0.05 Å. For comparison, molecular modeling of an all-trans conformation of $HO(CH_2)_9CHBr(CH_2)_{10}OH$ predicts that the bromine atom is located 14.8 Å from one end of the molecule and 13.5 Å from the other end of the molecule. In Figure 5, the position of the Br− functionality appears to alternate by 1.2 Å, consistent with its asymmetric location in the molecule and with disorder in the position of the bromine group within individual lamellae.

The bright STM region exhibited by the internal −Br group stands in contrast to the behavior previously reported for overlayers of 12-bromododecanol on HOPG, in which the region containing the −Br was observed to be dark relative to the methylene groups (the Br region had a mean length of 4.1 ± 0.1 Å and a mean height of -0.41 ± 0.05 Å).[24] Calculations suggest that this difference in image contrast between the terminal and internal −Br group is a consequence of topographic differences in the location of the functionality relative to the STM tip.[25] Parts A and B of Figure 6 show the simulated STM images for a terminal bromine in the trans and gauche conformations, respectively. For the trans conformation, the bromine atom is dark, but for the gauche conformation, the bromine atom is bright. These results are in excellent agreement with the experimental data reported herein.

4. STM Images of $H_3C(CH_2)_{16}CHBr(CH_2)_{16}CH_3$. Figure 7 presents the STM image of an alkane having an internal bromide functionality, 18-bromopentatriacontane, $H_3C(CH_2)_{16}CHBr(CH_2)_{16}CH_3$. The average molecular length is 48.8 ± 0.5 Å, compared to the expected length of 45.5 Å obtained from molecular modeling of the all-trans conformation of $H_3C(CH_2)_{16}CHBr(CH_2)_{16}CH_3$. The bright features in the image are attributed to the internal −Br groups and have a mean length of 10.6 ± 0.1 Å and a mean height of 2.86 ± 0.05 Å. As with the internal bromoalkanediol, the theoretical calculations are in excellent agreement with the experimental results (Figure 8), with the calculations predicting that regions around internal −Br groups are bright in STM images.

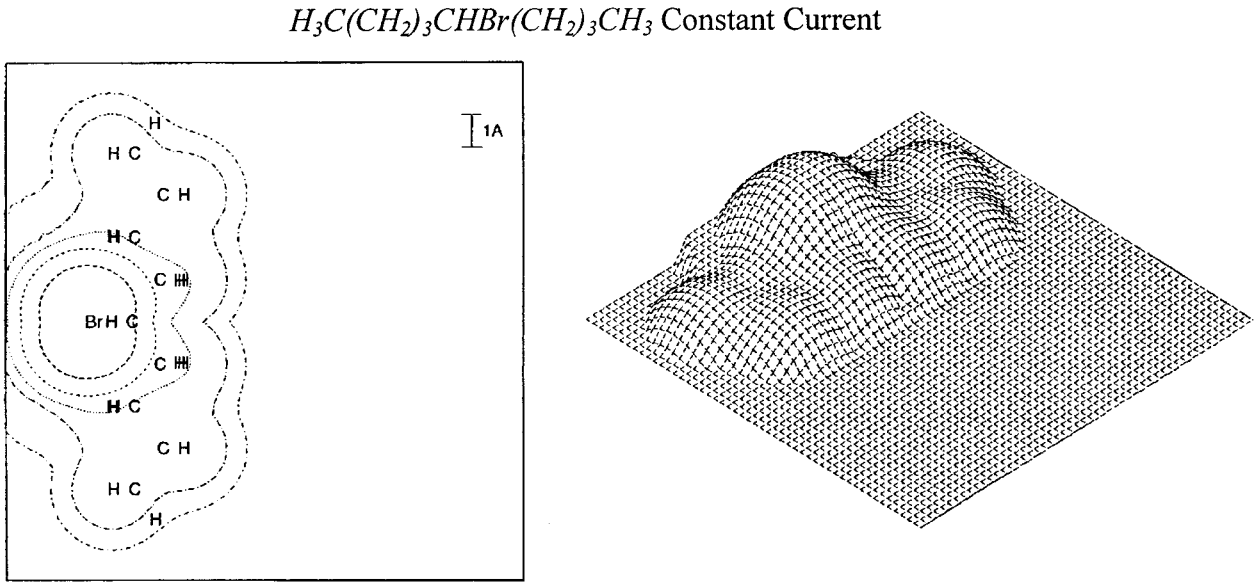

Figure 8. Calculated constant-current STM image for an internally substituted bromoalkane molecule laid flat on the graphite surface with the bromine heteroatom in a position pointing away from the graphite surface. Molecular modeling of $H_3C(CH_2)_{16}CHBr(CH_2)_{16}CH_3$ indicated that the −Br group is 1.1 Å higher than the methylene backbone of the molecule, while the STM simulation shown produces a 1.26 Å peak over the region of the methyl group.

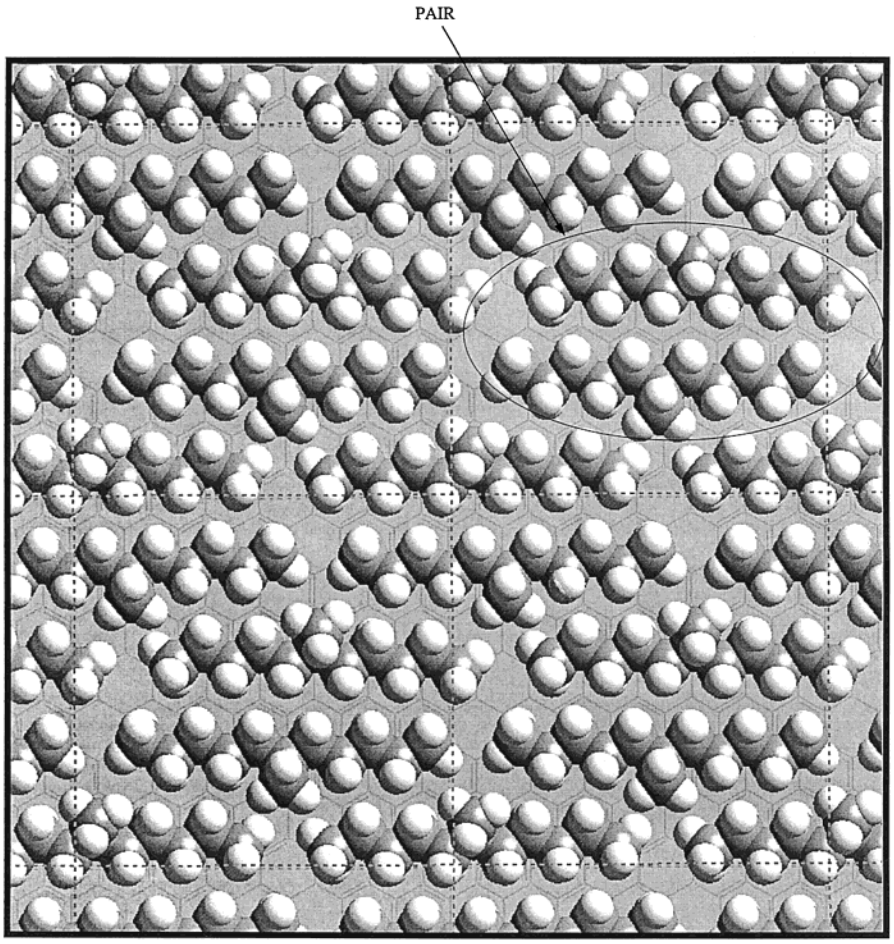

Figure 9. Schematic diagram of the proposed packing of the methylalkane molecules; $H_3C(CH_2)_4CHCH_3(CH_2)_4CH_3$ molecules are shown for clarity. Note that the packing angle θ is 0° in this configuration.

Despite the steric similarities between $-CH_3$ and $-Br$ groups, the $H_3C(CH_2)_{16}CHBr(CH_2)_{16}CH_3$ overlayers exhibit a different molecular packing arrangement than that displayed by $H_3C(CH_2)_{16}CHCH_3(CH_2)_{16}CH_3$ (cf. Figures 3 and 7). As observed for $H_3C(CH_2)_{16}CHCH_3(CH_2)_{16}CH_3$, $H_3C(CH_2)_{16}CHBr(CH_2)_{16}CH_3$ molecules in adjacent rows of abutting lamellae are aligned collinearly. However, for $H_3C(CH_2)_{16}CHBr(CH_2)_{16}CH_3$, the packing angle θ is observed to be 8° rather than the angle of 0° that is observed for overlayers of $H_3C(CH_2)_{16}CHCH_3(CH_2)_{16}CH_3$ and for overlayers of alkanes on graphite.

IV. Discussion

1. Relative Importance of Molecular Geometry and Topography on STM Image Contrast. The STM data described herein underscore the interplay between the topographic and electronic coupling factors that determine the local contrast observed in a STM image. The locations of bright spots in STM images of alkane and alkanol overlayers have been shown previously to be strongly correlated with the positions of the upward-pointing hydrogen atoms in the methylene units of these molecules.[24,25,34] Thus, topography plays an important role in determining the image contrast of such systems. However, for some of the functional groups observed previously,[24] electronic coupling factors appear to dominate the image contrast. For example, even though $-CF_3$ groups are large relative to methyl groups, they appear dark relative to methylene units in STM images of $CF_3(CH_2)_{11}OH$ or $CF_3(CF_2)_3(CH_2)_{10}OH$. Similarly, the amine functionality appears bright relative to internal methylene groups in dioctadecylamine, $(C_{18}H_{37})_2NH$ [24] and in $CH_3(CH_2)_{17}NH_2$,[22] even though the amine group is sterically smaller than the methylene regions of these molecules.

The results described herein demonstrate an even more subtle interplay between the topographic and electronic features of various functional groups. Bromide and $-OH$ groups were bright in STM images when these groups were located in internal positions on alkane chains (Figures 1, 3, 5, 7), whereas when these groups were placed in terminal positions on alkanol chains, they produced dark regions in the STM images.[24] The calculations and experimental results presented here for $-Br$ groups are in agreement with the image-contrast reversal that has been reported for terminal $-Br$ groups after sustained imaging of *n*-alkyl bromide overlayers on graphite.[23] These topographic and electronic effects can be understood, and in fact correctly predicted, from electronic structure calculations of the molecules studied to date. In this respect, the agreement between theory and experimental data on these systems is very encouraging. Thus, certain functional groups, such as thiols or thioethers, can potentially be used as markers to probe molecular topography in a variety of complex systems, including possibly oligonucleotides and other large molecules. However, the changes in sign, as well as in magnitude, of the STM image contrast of the $-OH$ and $-Br$ functional groups observed herein imply that, in these cases at least, identification of the composition and geometric arrangement of an unknown molecule from its STM image will be difficult without the use of supplemental information.

2. Intermolecular Interactions in the Substituted Alkane and Alkanol Overlayers. The STM images discussed above

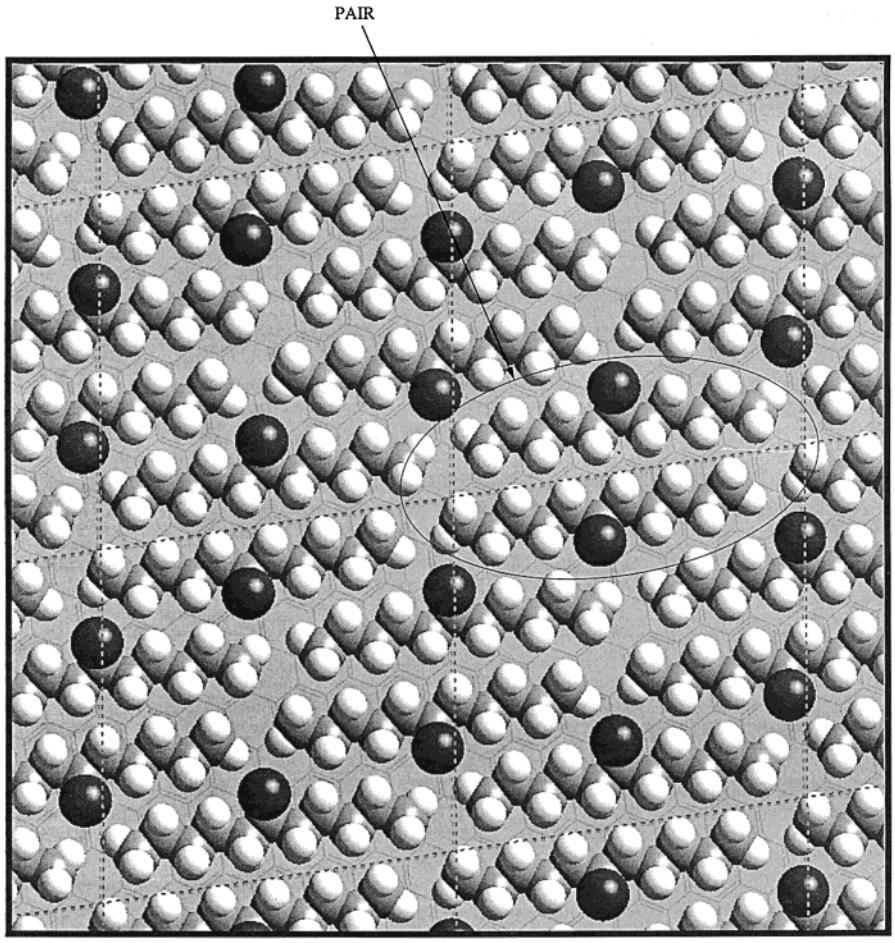

Figure 10. Schematic diagram of the proposed packing of the bromoalkane molecules; $H_3C(CH_2)_4CHBr(CH_2)_4CH_3$ molecules are shown for clarity. Note that the packing angle θ is 8° in this configuration.

reveal several different packing structures of the molecules both within and between the lamellae of the various overlayers. The intermolecular angle θ and the locations of the internal functional group markers in the molecules studied in this work provide useful metrics that allow investigation of these packing interactions.

The simplest packing arrangements can be readily understood from steric considerations. Alkane overlayers on graphite exhibit $\theta = 0°$, which is consistent with the tendency to maximize van der Waals interactions between neighboring molecules within a lamella.[24] This packing arrangement also minimizes steric repulsions between methylene hydrogen atoms on adjacent alkane chains. Additionally, repulsions between adjacent molecules in abutting lamellae are minimized by having these molecules stagger by $^1/_2$ a molecular width, and this feature is clearly observed in the STM images of such systems.[24] The internal −OH group in the molecule $H_3C(CH_2)_{16}CHOH(CH_2)_{16}CH_3$ studied in this work apparently did not induce sufficient steric repulsion between adjacent molecules in a lamella or offer the opportunity for sufficient hydrogen-bonding interactions within a lamella to perturb this basic packing structure; thus, the packing arrangement exhibited by $H_3C(CH_2)_{16}CHOH(CH_2)_{16}CH_3$ (Figure 1) is, within experimental error, identical to that exhibited by simple *n*-alkane overlayers on graphite.[24]

The next simplest packing arrangement has $\theta \approx 26°$. In this situation, adjacent molecules within a lamella sacrifice a van der Waals interaction and stagger by two full methylene units such that internal hydrogens on one chain fill hollows in the structure of the adjacent chain in a lamella.[24] The loss of the van der Waals interactions at one end of the alkyl chain either can be driven by a favorable hydrogen-bonding interaction between functional groups at the other terminus of the alkane chains, as evidenced by the observation that $\theta = 26°$ for alkanols on HOPG,[24] or can be driven by the tendency to avoid unfavorable interactions between functional groups in the centers of such chains, as presumably reflected in the value of $\theta = 26°$ that is exhibited by overlayers of $(C_{16}H_{33})_2O$ on HOPG.[24] The diol having an internal Br group, $HO(CH_2)_9CHBr(CH_2)_{10}OH$, was observed in this work (Figure 5) to pack in a fashion similar to that of other substituted and unsubstituted alkanols and displayed $\theta = 23°$. This packing therefore presumably reflects the strong tendency to obtain favorable hydrogen-bonding interactions at the termini of the molecules in the overlayer, and these interactions dominate any steric interactions within a lamella that might arise because of the presence of the internal −Br groups.

Other molecules studied in this work, however, exhibited different packing angles and different molecular arrangements within a lamella from those displayed by *n*-alkanes or *n*-alkanols. The $H_3C(CH_2)_{16}CHCH_3(CH_2)_{16}CH_3$ overlayer is one such system of interest. Figure 9 depicts a proposed packing scheme for this system that is consistent with the STM images of Figure 3. In this structure, adjacent molecules within a lamella form pairs, with molecules in each pair having their methyl groups staggered and pointing away from each other. Additionally, the methyl groups occupy troughs formed by the ends of similar molecules that are packed in an identical structure but that are located in abutting, adjacent lamellae. Finally, adjacent pairs of molecules in a given lamella are in translational registry with each other relative to the propagation direction of a lamella.

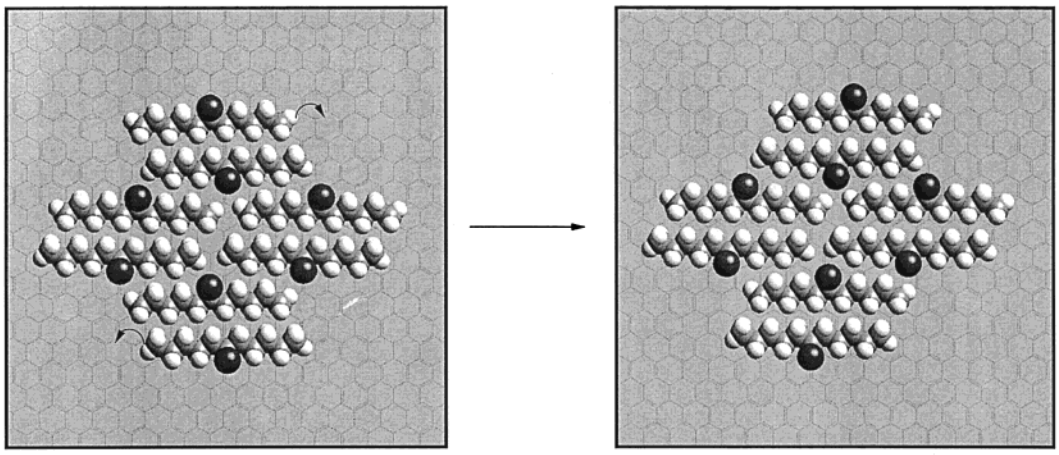

Figure 11. Schematic diagram showing the conversion between the proposed packing of $H_3C(CH_2)_{16}CHCH_3(CH_2)_{16}CH_3$ (left) and $H_3C(CH_2)_{16}CHBr(CH_2)_{16}CH_3$ (right) on graphite. For clarity, the molecules have been shortened in the figure to 11 carbon chains to allow the viewer to focus on the packing around the functional group regions. In addition, the diagram on the left has placed Br functional groups in positions that would be occupied by internal methyl groups in the $H_3C(CH_2)_{16}CHCH_3(CH_2)_{16}CH_3$ structure so that the interconversion between the packing of the $H_3C(CH_2)_{16}CHCH_3(CH_2)_{16}CH_3$ overlayer and that of the $H_3C(CH_2)_{16}CHBr(CH_2)_{16}CH_3$ can be seen by comparison of the two diagrams. Conversion of the packing of the $H_3C(CH_2)_{16}CHCH_3(CH_2)_{16}CH_3$ overlayer into that of the $H_3C(CH_2)_{16}CHBr(CH_2)_{16}CH_3$ layer can be achieved by translation of the outermost two molecules that form adjacent molecular pairs within a lamella by one $-CH_2-CH_2-$ distance normal to the vector that lies parallel to the propagation direction of the lamella, as indicated by the arrows in the diagram on the left.

This overlayer structure is consistent with the observations of a packing angle of $\theta = 0°$ (Figure 3).

An alternative structure for this system, in which the methyl groups of a given pair of molecules are directed toward one another rather than away from each other, with otherwise identical interlamellar packing parameters, can be ruled out from the STM data. The observed distance of 11.7 ± 0.3 Å between the pairs of bright spots in Figure 3 is in excellent agreement with the expected distance of 11.8 Å obtained from the packing arrangement of Figure 9, whereas if the methyl groups pointed toward each other, a much smaller methyl−methyl distance would be observed.

The differences in packing observed for this overlayer relative to the packing of simple alkane chains presumably arise because of steric interactions imposed by the presence of the internal methyl functionality. Although a search of the Cambridge structural database did not readily yield analogies to this structure in available crystal structures of internally substituted alkanes, the pairing motif revealed by the STM images of the system is clearly a low-energy packing arrangement for two-dimensional systems that have significant steric interactions arising from a functional group being located at an internal position on a trans conformation alkyl chain.

The substitution of an internal $-Br$ group for the internal $-CH_3$ group results in yet another molecular packing arrangement. Figure 10 displays a packing scheme that is consistent with the STM data for $H_3C(CH_2)_{16}CHBr(CH_2)_{16}CH_3$ overlayers on graphite (Figure 7). The pairing motif of adjacent molecules in a lamella displayed by $H_3C(CH_2)_{16}CHCH_3(CH_2)_{16}CH_3$ (cf. Figure 9) is also evident in this packing structure. As is the case for $H_3C(CH_2)_{16}CHCH_3(CH_2)_{16}CH_3$, the functional groups ($-Br$ in this case) for a given pair of molecules can be assigned to be directed away from one another because the measured distance of 7.8 ± 0.3 Å is in excellent agreement with the expected distance of 7.6 Å.

Interestingly, the packing structure for $H_3C(CH_2)_{16}CHBr(CH_2)_{16}CH_3$ differs from that of $H_3C(CH_2)_{16}CHCH_3(CH_2)_{16}CH_3$ with respect to the arrangement of the functional groups relative to each other at the level of second- and third-nearest-neighbor functional group interactions. This results in a distinctly different packing arrangement of the molecules both within a lamella and across abutting lamellae. One method to visualize the conversion of the packing of the $H_3C(CH_2)_{16}CHCH_3(CH_2)_{16}CH_3$ overlayer into that of the $H_3C(CH_2)_{16}CHBr(CH_2)_{16}CH_3$ layer involves translation of the outermost two molecules that form adjacent molecular pairs within a lamella. The translation occurs by one $-CH_2-CH_2-$ distance normal to the vector that lies parallel to the propagation direction of the lamella (Figure 11). This translation retains a staggered interaction between adjacent molecules that form pairs in the packing structure, but it also translationally offsets adjacent pairs of molecules in a lamella relative to the propagation vector of a lamella. Consistently, the packing of Figure 11 predicts an angle θ of 8°, in accord with the experimental observations for this system (Figure 7). Furthermore, such a packing arrangement results in a chiral overlayer domain because the mirror image of this structure exhibits $\theta = -8°$ relative to the propagation direction of a lamella.

The difference between the packing in the Br and Me cases is very subtle. The electrostatic energy difference between $H_3C(CH_2)_{16}CHBr(CH_2)_{16}CH_3$ molecules arranged in the packing arrangement of Figure 11 vs $H_3C(CH_2)_{16}CHBr(CH_2)_{16}CH_3$ molecules arranged in the $H_3C(CH_2)_{16}CHCH_3(CH_2)_{16}CH_3$ packing structure of Figure 10 is <1 kcal/mol. Additionally, Br and Me are conventionally thought to be sterically nearly identical. Investigations of the analogous compounds that contain $-Cl$ or $-F$ instead of $-Br$, as well as temperature-dependent experiments to evaluate the energetic differences between the two packing structures, would be especially interesting to address the subtleties that control these packing force issues in detail. In addition to elucidating features that control the image contrast of functional groups, STM studies of these systems thus offer an opportunity to examine, both theoretically and experimentally, the intermolecular interactions that dictate crystalline packing arrangements in two-dimensional overlayers.

V. Conclusions

STM images have revealed the interplay between the topographic and electronic coupling factors that determine the

local contrast of a functional group in an STM image. Bromide and −OH groups were bright in STM images when these groups were located in internal positions on alkane chains, whereas when these groups were placed in terminal positions on alkane chains, locally dark regions were observed in the STM images of such systems. These topographic and electronic effects can be understood, and in fact correctly predicted, from electronic structure calculations of the molecules studied to date. However, the changes in sign, as well as in magnitude, of the STM image contrast of the −OH and −Br functional groups observed herein imply that, in these cases at least, identification of the composition and geometric arrangement of an unknown molecule from its STM image will be difficult without the use of supplemental information. Additionally, STM has been shown to be a useful tool to investigate the different packing arrangements of adsorbates on a surface in equilibrium with the adsorbed molecules dissolved in solution phase.

Acknowledgment. We acknowledge the NSF, Grants CHE-9634152 (N.S.L.), CHE-95-22179 (W.A.G.), and ASC-92-17368 (W.A.G.) for partial support of this work.

References and Notes

(1) Frommer, J. *Angew. Chem., Int. Ed. Engl.* **1992**, *31*, 1298.
(2) Smith, D.; Hörber, J.; Binnig, G.; Nejoh, H. *Nature* **1990**, *344*, 641.
(3) Smith, D.; Hörber, J.; Gerber, C.; Binnig, G. *Science* **1989**, *245*, 43.
(4) Ludwig, C.; Gompf, B.; Glatz, W.; Petersen, J.; Eisenmenger, W. *Z. Phys. B.* **1992**, *86*, 397.
(5) Smith, D.; Heckl, W. *Nature* **1990**, *346*, 616.
(6) Ohtani, H.; Wilson, R.; Chiang, S.; Mate, C. *Phys. Rev. Lett.* **1988**, *60*, 2398.
(7) Lippel, P.; Wilson, R.; Miller, M.; Wöll, C.; Chiang, S. *Phys. Rev. Lett.* **1989**, *62*, 171.
(8) Hallmark, V.; Chiang, S.; Brown, J.; Wöll, C. *Phys. Rev. Lett.* **1991**, *66*, 48.
(9) Kim, Y.; Bard, A. *Langmuir* **1992**, *8*, 1096.
(10) Smith, D.; Bryant, A.; Quate, C.; Rabe, J.; Gerber, C.; Swalen, J. *Proc. Natl. Acad. Sci. U.S.A.* **1987**, *84*, 969.
(11) McMaster, T.; Carr, H.; Miles, M.; Cairns, P.; Morris, V. *Macromolecules* **1991**, *24*, 1428.
(12) Yang, R.; Naoi, K.; Evans, D.; Smyrl, W.; Hendrickson, W. *Langmuir* **1991**, *7*, 556.
(13) Wilson, R.; Meijer, G.; Bethune, D.; Johnson, R.; Chambliss, D.; de Vries, M.; Hunziker, H.; Wendt, H. *Nature* **1990**, *348*, 621.
(14) Li, Y.; Chander, M.; Patrin, J.; Weaver, J.; Chibante, L.; Smalley, R. *Science* **1991**, *253*, 429.
(15) Allen, M.; Ballooch, M.; Subbiah, S.; Tench, R.; Siekhaus, W.; Balhorn, R. *Scanning Microsc.* **1991**, *5*, 625.
(16) Youngquist, M.; Driscoll, R.; Coley, T.; Goddard, W.; Baldeschwieler, J.; *J. Vac. Sci. Technol. B* **1991**, *9*, 1304.
(17) Lu, X.; Hipps, K. W.; Wang, X. D.; Mazur, U. *J. Am. Chem. Soc.* **1996**, *118*, 7197.
(18) Sautet, P.; Joachim, C. *Ultramicroscopy* **1992**, *42A*, 115−121.
(19) Sautet, P.; Joachim, C. *Surf. Sci.* **1992**, *271*, 387−394.
(20) Fisher, A. J.; Blochl, P. E. *Phys. Rev. Lett.* **1993**, *70*, 3263−3266.
(21) Venkataraman, B.; Flynn, G. W.; Wilbur, J. L.; Folkers, J. P.; Whitesides, G. M. *J. Phys. Chem.* **1995**, *99*, 8684.
(22) Cyr, D. M.; Venkataraman, B.; Flynn, G. W.; Black, A.; Whitesides, G. M. *J. Phys. Chem.* **1996**, *100*, 13747.
(23) (a) Cyr, D. M.; Venkataraman, B.; Flynn, G. W. *Chem. Mater.* **1996**, *8*, 1600. (b) Fang, H.; Giancarlo, L.; Flynn, G. W. *J. Phys. Chem. B* **1998**, *102*, 7421. (c) Giancarlo, G.; Cyr, D.; Muyskens, K.; Glynn, G. W. *Langmuir* **1998**, *14*, 1465. (d) Giancarlo, G. C.; Fang, H.; Rubin, S. M.; Bront, A.; Flynn, G. W. *J. Phys. Chem., B* **1998**, *102*, 10255.
(24) Claypool, C. L.; Faglioni, F.; Goddard, W. A., III; Gray, H. B.; Lewis, N. S.; Marcus, R. A. *J. Phys. Chem. B* **1997**, *101*, 5978.
(25) Faglioni, F.; Claypool, C. L.; Lewis, N. S.; Goddard, W. A., III. *J. Phys. Chem. B* **1997**, *101*, 5996.
(26) McGonigal, G. C.; Bernhardt, R. H.; Thomson, D. J. *Appl. Phys. Lett.* **1990**, *57*, 28.
(27) McGonigal, G. C.; Bernhardt, R. H.; Yeo, Y.; Thomson, D. J. *J. Vac. Sci. Technol. B* **1991**, *9*, 401.
(28) Rabe, J. P.; Buchholz, S. *Science* **1991**, *253*, 424.
(29) Buchholz, S.; Rabe, J. P. *J. Vac. Sci. Technol. B* **1991**, *2*, 1126.
(30) Buchholz, S.; Rabe, J. P. *Angew. Chem., Int. Ed. Engl.* **1992**, *31*, 189.
(31) Cincotti, S.; Rabe, J. P. *Appl. Phys. Lett.* **1993**, *62*, 3531.
(32) Yeo, Y. H.; McGonigal, G. C.; Thomson, D. J. *Langmuir* **1993**, *9*, 649.
(33) Rabe, J. P.; Buchholz, S.; Askadskaya, L. *Synth. Met.* **1993**, *54*, 349.
(34) Liang, W.; Whangbo, M. H.; Wawkuschewski, A.; Cantow, H. J.; Magonov, S. N. *Adv. Mater.* **1993**, *5*, 817.
(35) (a) Hatta, I.; Nishino, J.; Sumi, A.; Hibino, M. *Jpn. J. Appl. Phys.* **1995**, *34*, 610. (b) Yoshimura, K.; Arakawa, H.; Ikai, A. *Jpn. J. Appl. Phys.* **1996**, *35*, 3754.
(36) Bard, A. J.; Chang, H. *J. Am. Chem. Soc.* **1990**, *112*, 4698.
(37) Mayo, S. L.; Olafson, B. D.; Goddard, W. A., III. *J. Phys. Chem.* **1990**, *94*, 8897.
(38) *Gaussian 92/DFT*, revision F.4; Gaussian Inc.: Pittsburgh, PA, 1993. *Gaussian 94*, revision B.3; Gaussian Inc.: Pittsburgh, PA, 1995.